Mode interaction in a forced homogeneous jet at low Reynolds numbers

By I. Danaila[1] AND B. J. Boersma

The near-field evolution of a forced axisymmetric jet was investigated by means of Direct Numerical Simulation (DNS). The numerical configuration simulated a low Reynolds number jet ($Re_D = 1500$) issuing from a circular orifice in a solid wall. Periodic streamwise velocity disturbances were applied at the nozzle. Four modal distributions of forcing were studied. The first and the second type of perturbation contained only one of the two fundamental instability modes of the round jet: the *axisymmetric* $m = 0$ mode and the *helical* $m = 1$ mode. A 'classical' evolution of the jet flow was obtained for these cases. This provided a reference to the third case, which consisted of forcing simultaneously the counter-rotating helical modes $m = \pm 1$ with the same amplitude and the same frequency (*flapping mode*). The jet split into two branches, taking a distinct 'Y' shape characteristic of the *bifurcating jets* (cf. Lee & Reynolds, 1985). A different evolution of the bifurcating jet is observed when superposing the axisymmetric mode, at the most amplified unstable frequency, with the flapping mode, with the same amplitude but with subharmonic frequency. This combination led to resonant growth of the jet with a spectacular increase of the spreading angle up to 90^o.

1. Introduction

Considering the many practical applications of round jets (aeroacoustic, combustion, propulsion, mixing), numerous attempts have been made to control jet mixing and entrainment. A full listing of the proposed control approaches would easily exceed one hundred references.

All the control techniques use active or passive devices to alter the vortex dynamics close to the nozzle. From a theoretical point of view, the large coherent structures characterizing the near field evolution can be assimilated with instability modes, described by their azimuthal wavenumber m. Several fundamental results derived from linear stability analysis and experimental observations offer a complete picture of the mode selection in the near field of a *natural* (unforced) axisymmetric jet:

(i) The two linearly dominating modes are the axisymmetric (or varicose, $m = 0$) and first helical ($m = 1$) modes. For jets with thin initial shear layer, the linear amplification characteristics of these two fundamental modes are similar (e.g. Batchelor & Gill 1962, Michalke 1982). This has been confirmed in experiments (e.g. Cohen & Wygnanski 1987, Corke *et al.* 1991).

1 I. R. P. H. E., 12 Av. Général Leclerc, 13003 Marseille, France.

(ii) Higher helical modes ($m \geq 2$) are always less amplified than the fundamental modes (Mattingly & Chang 1974, Plasko 1979) and were rarely (if ever) observed in experiments.

(iii) Although the linear characteristics of the fundamental modes are almost identical, only one mode ($m = 0$ or $m = 1$) will dominate at the early stages of the near field evolution. The dominant mode is selected by amplification of coherent initial perturbations such as the pressure field at the lip (Morris 1976). In most laboratory jets, only planar disturbances are emanating from the nozzle and, consequently, the axisymmetric mode plays the dominant role (Cohen & Wygnanski 1987b). If the disturbances at the jet exit lip are stochastic, the switch from one mode to the other can occur, but the two fundamental modes never exist together (Corke *et al.* 1991).

(iv) Since the linear stability characteristics of the counter-rotating helical modes $m = 1$ and $m = -1$ are indistinguishable (Batchelor & Gill 1962, Danaila *et al.* 1998), there is a greater likelihood to observe both $m = \pm 1$ modes in the flow rather than a single helical mode. The nonlinear interaction of these two modes lead to characteristic flow patterns (Dimotakis *et al.*, 1983, Danaila *et al.* 1997). When the $m = \pm 1$ modes have the same frequency and amplitude, the so-called *flapping mode* is obtained (see, for example, Morrison & McLaughlin 1980). In conclusion, the linear superpositions of the $m = \pm 1$ modes (in particular the flapping mode) can also be considered as fundamental modes.

In the light of these results, the jet control techniques can be watched as attempts either to control the dynamics of a single fundamental mode or to force simultaneously several of these modes:

(1) The evolution of the axisymmetric mode characterized by vortex ring roll-up offers many possibilities of control. Many researchers have investigated the effects of axial acoustic forcing on the vortex ring generation (Crow & Champagne 1971, Bouchard & Reynolds 1982), spacing and pairing (Hussain & Zaman 1980, Hussain & Clark 1981, Ho & Huang 1982). The amplitude and frequency of the forcing excitation can determine the number of pairings and their locations and, consequently, the spreading rate of the jet. The azimuthal instability of rings and the formation of streamwise vortex filaments were reported as an important entrainment mechanism in jets (Liepmann & Gharib 1992). When combined with axial acoustic disturbances, passive azimuthal forcing (obtained by using corrugated nozzles) could be very effective in mixing and entrainment enhancement (Lasheras *et al.* 1991).

(2) The helical modes $m = \pm 1$ can be generated by controlled acoustic excitation (Parekh & Reynolds 1988, Corke & Kusek 1993) or triggered by passive devices which break the axial symmetry (e.g. tabs - Bradbury & Khadem 1975, sawtooth nozzles - Longmire & Duong 1995). Although less studied than the axisymmetric mode, the helical modes showed some interesting mixing properties. Mankbadi & Liu (1981) showed that helical modes are more efficient than the axisymmetric one in pumping energy into turbulent small scales due to its shorter streamwise lifespan. The subharmonic resonance of the $m = \pm 1$ modes can lead to a net increase (300%) of the jet momentum thickness compared to the unforced jet (Corke & Kusek 1993).

(3) The most interesting mixing and entrainment properties are obtained when combined axial and helical forcing are used. Lee & Reynolds (1985) used axial acoustic excitation to generate vortex rings and moved the nozzle in a circular path perpendicular to the jet axis (*orbital excitation*). Neighboring generated rings are radially shifted in different azimuthal planes and induce one another to move on distinct branches. The ratio R between the axial and the orbital forcing frequency set the number of branches. *Bifurcating* ($R = 2$), *trifurcating* ($R = 3$), and *blooming* ($1.6 < R < 3.2$ and non-integer) jets are obtained with a spectacular increase of the spreading angle (from 18^o for the unforced jet up to 80^o for the bifurcating jet). Parekh, Leonard & Reynolds (1988) obtained high Reynolds bifurcating jets using axial and flapping acoustic excitation produced by four speakers placed around the perimeter of the nozzle exit. The bifurcation occurred above a critical forcing amplitude, increasing with the Reynolds number. Higher forcing frequencies yielded bifurcating jets with larger spreading angles.

Similar (albeit more distorted) bifurcating jets were reported in jet experiments using axial forcing and passive control devices. Stepped or sawtooth trailing edges attached at the nozzle exit (Longmire & Duong 1995) or inclined nozzles (Webster & Longmire 1997) generated complex helical structures which altered the downstream evolution of vortex rings. The bifurcating effect was found to be strongest when low forcing frequencies were used, a trend opposite to that seen by Lee & Reynolds (1985). Zaman, Reeder & Samimy (1996) used a combination of two diametrically opposed tabs placed at the nozzle exit to obtain bifurcating supersonic jets. Further work (Zaman & Raman 1997) showed that, in low Mach number jets, tabs and axial excitation independently increased jet spreading while a combination of the two had an opposite effect.

This study was especially inspired by the experiments of Parekh *et al.* (1988), who studied the effects on the round jet evolution of four types of acoustic excitation: axisymmetric, helical, flapping, and *bifurcating* (i.e. axial + flapping). The spectacular increase in spreading of the bifurcating jet was compared to the reference cases provided by the axially and helically excited jets. One of the main conclusions of this study was the independence of the bifurcation phenomenon of the Reynolds number. For the explored range of high Reynolds numbers ($10\,000 < Re < 100\,000$), an optimum set of parameters (frequency and amplitude of excitation) can be found in order to obtain bifurcating jets similar to those reported by Lee & Reynolds (1985) for low Reynolds numbers ($2\,800 < Re < 10\,000$).

This observation suggests that bifurcating phenomena can be approached by Direct Numerical Simulation (DNS). Recent DNS of spatially evolving low Reynolds number jets proved very effective in investigating properties of the transitional (Danaila *et al.* 1997) or turbulent (Boersma *et al.* 1998) regimes of free incompressible jets. In this work we make use of DNS to assess the influence of the four abovementioned excitations on the jet evolution. Although the vortex dynamics of some bifurcating jets can be simulated by simpler numerical approaches, as the vortex filaments method (see Parekh *et al.* 1988), DNS is expected to offer a complete description of the underlying mechanisms involved in such flows.

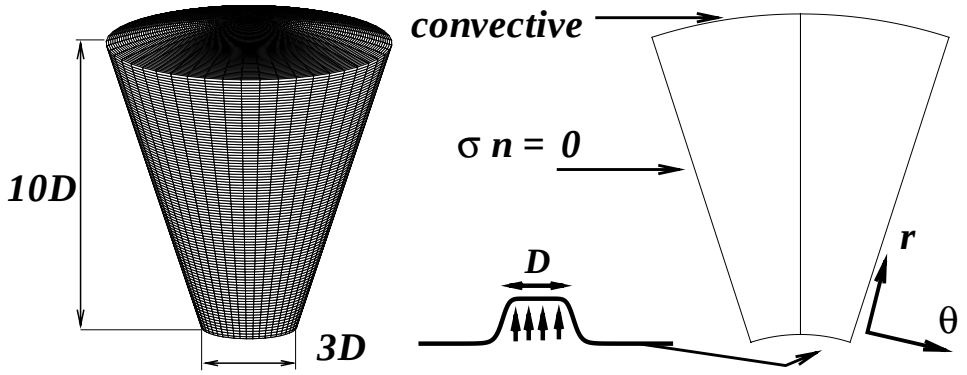

FIGURE 1. Computational domain and boundary conditions.

2. Numerical details

The numerical solver simulates a free round jet issuing from a circular orifice of diameter D in a solid wall. The solver solves the incompressible Navier-Stokes equations in a spherical coordinate system with (r, θ, ϕ) denoting the radial, azimuthal, and tangential directions. Details of the numerical scheme can be found in Boersma *et al.* (1998). The computational domain shown in Fig. 1 results from the intersection between the shell defined by the surfaces $r = 5D$ and $r = 15D$ and the cone starting from the center of the sphere with an opening angle of 36^o. The obtained geometry covers a domain with a streamwise extent of $15D$ and a spanwise diameter of $3D$ for the inflow section and $10D$ for the outflow section. Such a discretization is able to follow the streamwise spreading of the jet and allows a well-balanced resolution of the flow field with a reasonable number of grid points. For convenience, the cylindrical coordinates (r_c, θ_c, z) with r_c the radial, θ_c the azimuthal, and z the axial directions will be used to analyze the results.

The boundary conditions are also illustrated in Fig. 1. At the inflow section, the mean streamwise velocity profile is imposed as initial and boundary condition. We used the 'classical' hyperbolic tangent (*tanh*) profile, which matches very well with profiles measured in experiments (see Michalke 1984). In cylindrical coordinates it reads:

$$V_{z0}(r_c)/V_0 = 0.5\{1 + \tanh[0.25D/\Theta_0(D/(4r_c) - r_c/D)]\}, \qquad (1)$$

where V_0 is the centerline velocity (at $r_c = 0$) and Θ_0 the initial momentum thickness. At the lateral boundary, traction-free boundary conditions are used (see, for example, Gresho 1991): $\sigma_{ij} \cdot n_j = 0$, where σ_{ij} is the stress tensor and n_j the unit normal on the boundary. The main advantage of this traction-free condition over the largely used free-slip or no-slip boundary conditions is that fluid exchange across the boundary is allowed. This appeared to be very useful to properly simulate the entrainment of ambient fluid in the spreading jet flow. A so-called convective boundary condition (Orlanski 1976, Lowery & Reynolds 1986) was used to evacuate the vortex structures through the downstream boundary. This condition is numerically stable but physically not very realistic in elliptic flows. However, the convective nature of the homogeneous jet flow (Huerre & Monkewitz 1990) allows it to eventually evacuate spurious reflections at the outflow boundary.

3. Selection of physical parameters

The guidelines for the selection of physical parameters used in our spatial simulation were found in Parekh *et al.* (1988). In their experiments, the Reynolds number was varied in the range $10^4 < Re_D = V_0 D/\nu < 10^6$. The measured ratio between the jet diameter and the momentum thickness of the inflow mean velocity profile was $D/\Theta_0 = 66$ for $Re_D = 10^4$ and about seven times larger for $Re_D = 10^6$. The acoustic excitation was characterized by the axial Strouhal number $St_a = f_a D/V_0$ when the axisymmetric mode was forced at the frequency f_a. The corresponding helical Strouhal number $St_h = f_h D/V_0$ was defined for the helical or flapping mode excitation. The dual-mode excitation was characterized in terms of the frequency ratio $R_f = f_a/f_h$ and the axial Strouhal number St_a.

The bifurcating jet was obtained only if $R_f = 2$ and for a well defined range of axial Strouhal numbers: $0.4 < St_a < 0.7$. Nevertheless, the maximum jet spreading occurred around $St_a = 0.55$ for all investigated Reynolds numbers. The same optimum value for St_a was reported by Lee & Reynolds (1985) for the bifurcating jet at $Re_D = 3700$. No satisfactory explanation of this phenomenon was provided. We believe that the invariance of St_a with the Reynolds number can be connected to another unexplained phenomenon reported in free jets, which is the locking of the jet *preferred* Strouhal number for large ratios D/Θ_0 (see Ho & Huerre 1984). Indeed, it is well known that the most amplified frequency at the end of the potential core is independent of the Reynolds number and results from nonlinear interactions (Crow & Champagne 1971). The value of the Strouhal number based on this preferred frequency and the jet diameter varies from one experiment to another between 0.2 and 0.5 (Gutmark & Ho 1983). The preferred Strouhal number scales with the shear-layer frequency for small D/Θ_0 and 'locks' at a constant value of 0.44 for $D/\Theta_0 \geq 240$ (Ho & Huerre 1984). A similar phenomenon can occur in high Reynolds bifurcating jets, where collective interactions of vortex rings at the end of the potential core cause the jet to split in two distinct branches. Consequently, the value $St_a = 0.55$ can be considered as the preferred axial Strouhal number of the bifurcating jets characterized by large ratios D/Θ_0.

In view of these experimental observations, we chose the following physical parameters to define the inflow velocity profile given by Eq. (1): $D/\Theta_0 = 60$ and $Re_D = 1500$. For this low Reynolds number, a uniform mesh of $(192 \times 128 \times 96)$ grid-points in the (r, θ, ϕ) directions is sufficient to resolve the smallest scales of the motion in the considered computational domain (see Boersma *et al.* 1998). As a result of this discretization, 12 grid-points are situated in the initial shear region at the nozzle, offering a correct resolution of the instability waves.

The simulated jet is forced by superposing oscillating components on the mean nozzle exit velocity. Only streamwise velocity disturbances are used. The analytical form of the resulting inflow velocity profile is:

$$V_z(r_c, t) = V_{z0}(r_c)\left[1 + \sum_m A_m \sin\left(2\pi \frac{St_m V_0}{D} t - m\theta_c\right)\left(\frac{2r_c}{D}\right)^{|m|}\right], \qquad (2)$$

where V_{z0} is given by Eq. (1) and m is the azimuthal wavenumber of the excitation.

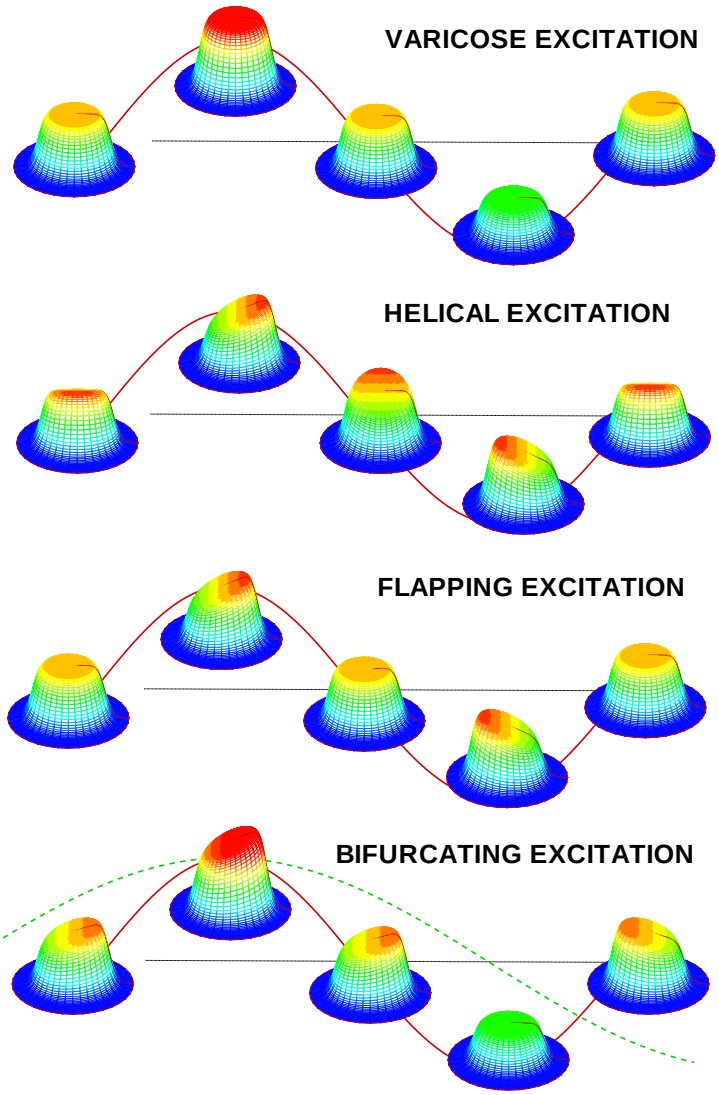

FIGURE 2. Three-dimensional representation of the streamwise velocity profile at the nozzle. Evolution during one cycle of excitation.

Four types of excitation were considered, as in experiments. The time evolution of the inflow velocity profile during one cycle of excitation can be followed in Fig. 2.

[(A)-jet] Axisymmetric excitation ($m = 0$); $St_a = 0.55$; $A_a = 0.15$.

The up and down 'movement' of the velocity profile around the mean value (Fig. 2) mimics the perturbation introduced by a speaker placed in the plenum chamber of a laboratory jet. The excitation parameters (St_a, A_a) were fixed in order to provide a reference case for the bifurcating jet (see below).

[(H)-jet] Helical excitation ($m = 1$); $St_h = 0.55$; $A_h = 0.15$.

This perturbation approaches the disturbances produced by an azimuthal array of acoustic drivers placed close to the jet lip and controlled by a helical input (Parekh *et al.* 1988, Corke & Kusek 1993). The asymmetric velocity profile makes a complete rotation during one period of excitation.

[(F)-jet] Flapping excitation $[(m=1)+(m=-1)]$; $St_f = 0.55$; $A_f = 0.15$.

The flapping excitation results from the superposition of the counter-rotating helical modes with the same amplitude and frequency. An equivalent form of the inflow velocity profile (Eq. 2) is in this case:

$$\frac{V_z(r_c,t)}{V_{z0}(r_c)} = \left[1 + A_f \sin\left(2\pi \frac{St_f V_0}{D} t\right) \cos(\theta_c) \left(\frac{2r_c}{D}\right)\right] \tag{3}$$

Compared to the helical excitation, the time evolution of the velocity profile (Fig. 2) is phase locked in the plane $\theta_c = 0$.

[(BF)-jet] Bifurcating excitation $[(m=0)+(m=1)+(m=-1)]$; $St_a = 0.55$; $St_f = St_a/2$; $A_a = A_f = 0.15$.

The bifurcating perturbation is obtained by imposing a dual-mode (axisymmetric + flapping) and dual-frequency ($R_f = St_a/St_f = 2$) excitation. Since both the experiments of Lee & Reynolds (1985) and Parekh *et al.* (1988) indicated a maximum spreading of the bifurcating jet for an axial Strouhal number of 0.55, the same value is considered here. The large excitation amplitude (15%) is close to that used by Lee & Reynolds (1985). Along with the amplitude, the relative phase (Φ) between the axial and the flapping excitations is very important. Bifurcation occurs only if the peak of the axial signal is approximately aligned with the peak of the flapping signal (Parekh *et al.* 1988). The measured values were $\Phi = 47^o \pm 15^o$ at $Re_D = 10^6$ and $\Phi = 31^o \pm 15^o$ at $Re_D = 50 \cdot 10^3$. In our simulations, we imposed the theoretical value $\Phi = 45^o$ to obtain the peak alignment (see the last frame of Fig. 2, with the dashed line representing the flapping component of the perturbation). The final form of the velocity profile can be written as:

$$\frac{V_z(r_c,t)}{V_{z0}(r_c)} = \left[1 + A_a \sin\left(2\pi \frac{St_a V_0}{D} t\right) + A_f \sin\left(2\pi \frac{St_f V_0}{D} t + \Phi\right) \cos(\theta_c) \left(\frac{2r_c}{D}\right)\right] \tag{4}$$

4. Results

The response of the jet flow to the excitations described above is analyzed both instantaneously and statistically. As in experiments, flow visualization is emphasized. For this purpose, a passive scalar conservation equation with Fickian diffusion assumption is solved with the same numerical scheme. Two different types of scalar injection are considered. The first scalar (S1) has the same mean inflow profile as the injection velocity (Eq. 1). This tracer marks all the jet fluid and provides a qualitative estimation of the entrainment through the interface between ambient and jet fluid. The second tracer (S2) is injected with a mean profile corresponding to the vorticity profile of the initial shear-layer (derivative of Eq. 1). This is useful to mark the vorticity-bearing jet mixing-layer and to track large coherent structures. For our numerical tracers, a very small diffusivity was chosen in order to avoid rapid contamination of all the computational domain. This is good assumption for water flow visualization, where the viscous diffusion of the (fluorescein) dye can be neglected.

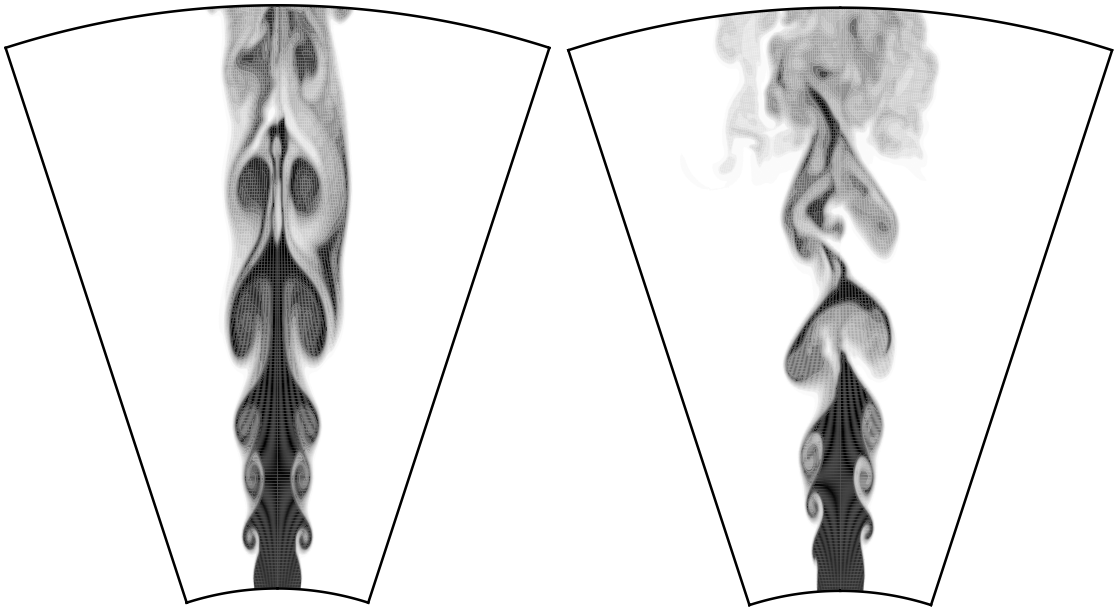

FIGURE 3. (A)-jet (left) and (H)-jet (right). Instantaneous cross-section ($\theta_c = 0$) in the (S1) passive scalar field.

4.1 Axisymmetric and helical excitations

Instantaneous cross-sections in the scalar field (S1) are displayed in Fig. 3 for the axially (left) and helically (right) excited jets. The large forcing amplitude expedites the transition of the the initially laminar jet mixing layers. In both cases the transition consists of formation of coherent structures of Kelvin-Helmholtz type (*cat-eyes*). These structures are spatially organized in toroidal vortex rings in case (A) and helical patterns in case (H).

It should be noted that, for the hyperbolic tangent velocity profile (1) with $D/\Theta_0 = 60$, the linear stability analysis (Michalke 1984) showed that the axisymmetric and the helical modes have almost the same 'most amplified' (or 'natural') frequency (f_n). In terms of Strouhal number based on the momentum thickness, its theoretical value is: $St_{\Theta_0} = f_n\,\Theta_0/V_0 = 0.017$. The corresponding Strouhal number based on the jet diameter will be $St_D = 1.02$. As a result, the forcing frequency ($St_a = St_h = 0.55$) is very close to the subharmonic 'natural' frequency and will cause 'collective interactions' of vortex structures (Ho & Huang 1982). Figure 3 also captures the vortex rings pairing process in the axially excited jet. For the helically excited jet, the coalescence of two neighboring vortex loops of the helix can be observed (Fig. 3). This phenomenon was never reported in experiments with a single helical mode input. A similar 'helical pairing' process was reported by Corke & Kusek (1993) in their jet, simultaneously forced with $m = \pm 1$ modes.

In both jets, vortex amalgamations generate larger coherent structures and increase the local momentum thickness of the shear layer. The streamwise wavelength is doubled by pairings as illustrated in Fig. 4 presenting a snapshot of the (S2) tracer evolution near the nozzle. The vortex cores are easily identified by high tracer

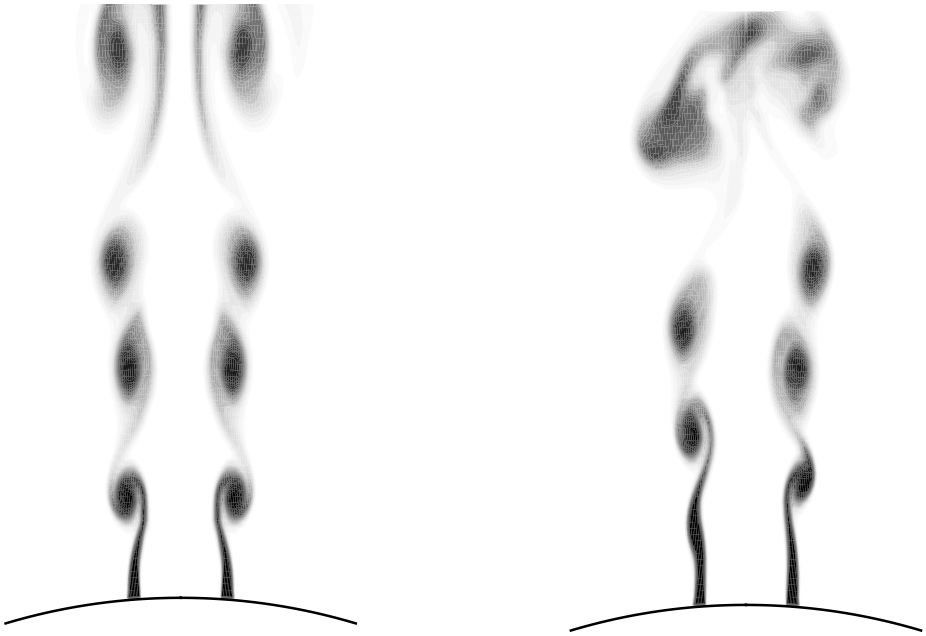

FIGURE 4. (A)-jet (left) and (H)-jet (right). Instantaneous cross-section ($\theta_c = 0$) in the (S2) passive scalar field. Zoom in the region close to the nozzle.

concentrations. From this visualization, the instability wavelength is estimated to $\lambda_a/D \approx 1.03$ for the case (A) and $\lambda_h/D \approx 0.86$ for the case (H). As the forcing frequency is higher than $f_n/2$, the response frequency of the shear will be equal to the forcing frequency (Ho & Huerre 1984). With this assumption, the convection velocity of the unstable modes can be calculated as $V_c/V_0 = \lambda/D\, St_D$. The obtained values $(V_c/V_0)_a = 0.56$ and $(V_c/V_0)_h = 0.47$ are very close to the theoretical value of 0.5.

Different azimuthal sections offer similar images for both cases. Figure 5 presents a three-dimensional picture of the large coherent structures dominating the near-field. The fundamental ($m = 0$) and ($m = 1$) unstable modes are clearly identified by means of iso-surfaces of low pressure (see Jeong & Hussain 1995).

However, the azimuthal symmetry of the axially forced jet is broken downstream of the pairing location. Stretched lateral ejection of the passive scalar (Fig. 3) suggests that secondary azimuthal instability develops and forms side-jets (see Liepmann & Gharib 1992). The azimuthally distorted structure of the last vortex ring displayed in Fig. 5 confirms this observation. Subsequent simulation of the axially forced jet with additional low amplitude (2%) white noise disturbances at the nozzle showed a more rapid breakup of the vortex rings into turbulent puffs beyond $z/D \approx 5$ (pictures not shown here). On the other hand, the helical structure is less stable and breaks up in small eddies without any additional disturbances (Fig. 3). This observation matches the results of Mankbadi & Liu (1981), showing that helical modes have a shorter streamwise lifespan than the axisymmetric mode. This property makes the helical modes more effective in transferring energy into small turbulent scales.

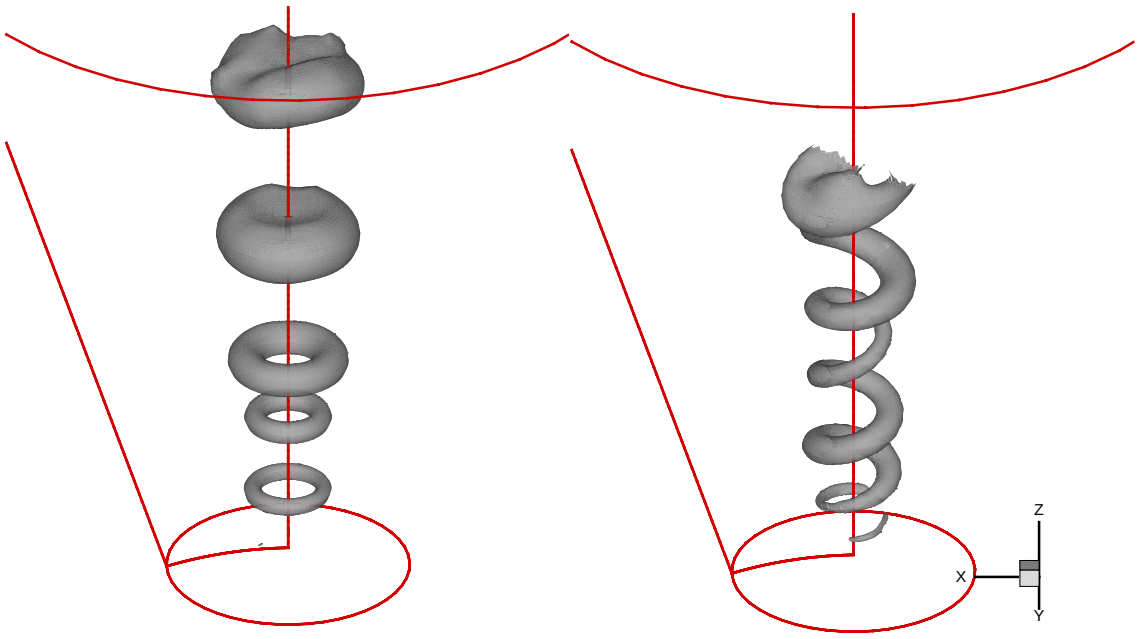

FIGURE 5. (A)-jet (left) and (H)-jet (right). Identification of large coherent structures by instantaneous iso-surfaces of low pressure ($p = 0.2 \cdot p_{min}$).

4.2 Flapping and bifurcating excitations

The structure of the simulated jet changes dramatically when flapping or bifurcating excitation are applied at the nozzle. A spectacular increase of the jet spreading angle is observed in the *bifurcating plane*. This plane of maximum spreading is fixed by the azimuthal position where the flapping perturbation locks ($\theta_c = 0$ in our case). The plane perpendicular to the bifurcation plane is also called *bisecting plane*. Figure 6 depicts instantaneous pictures of the (S1) scalar evolution in the bifurcating plane for the jet with flapping (left) and bifurcating (right) perturbation. The same picture taken in the bisecting plane is presented in Fig. 7. Both jets exhibit different behavior in the two planes.

In the bifurcating plane, the flapping excitation causes the jet to split into two distinct branches (Fig. 6-left). Approximately at the same downstream location ($z/D \approx 5$), the jet with bifurcation excitation spreads in a wide-angle turbulent structure (Fig. 6-right). In the bisecting plane, the scalar evolution is similar for both jets. The tracer, organized in large axisymmetric structures, seems to disappear downstream of $z/D \approx 5$ (Fig. 7). Practically no spreading is observed in this plane.

This different evolution in two perpendicular planes is a characteristic of experimentally observed bifurcating jets. Nevertheless, only the (F)-jet displays the Y-shaped structure, reported as the most striking feature of bifurcating jets at low Reynolds numbers ($Re_D \leq 10\,000$). On the other hand, the (BF)-jet shares features of the higher Reynolds number experimental bifurcating jets (see Lee & Reynolds 1985 and Parekh *et al* 1988). This is a surprising result, suggesting that new mechanisms are involved in our simulated jets.

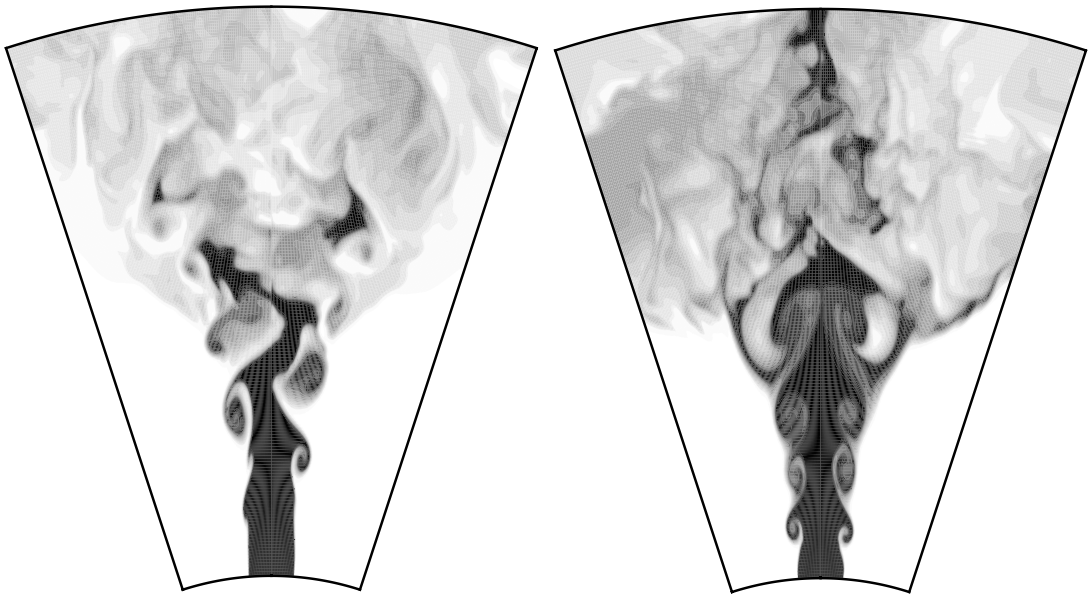

FIGURE 6. (F)-jet (left) and (BF)-jet (right). Instantaneous snapshot of the (S1) passive scalar field in the bifurcating plane ($\theta_c = 0$).

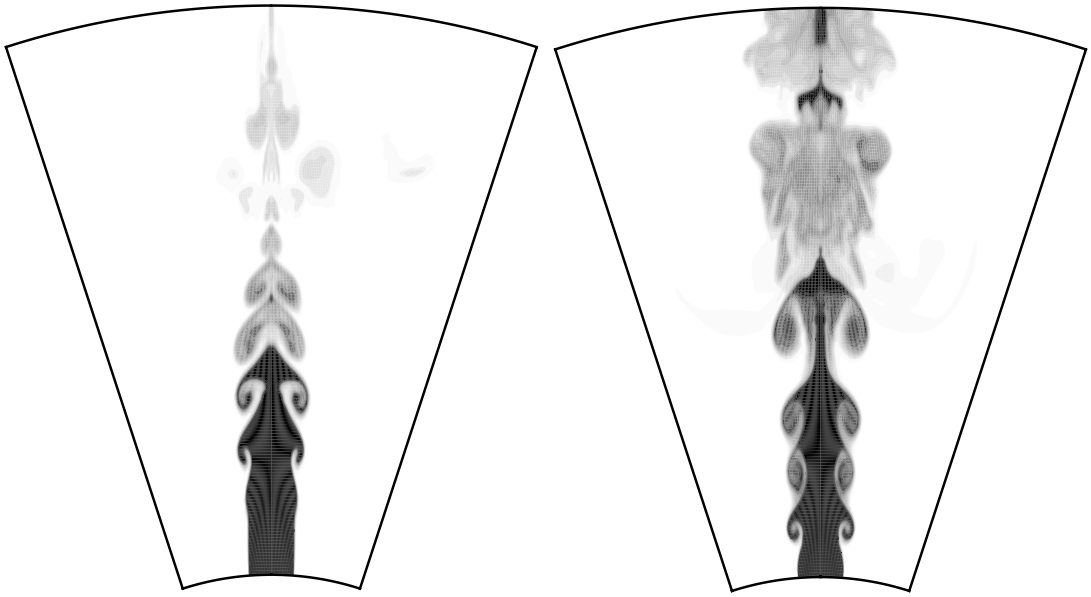

FIGURE 7. Same caption as in Fig. 6. Evolution in the bisecting plane ($\theta_c = 90$).

In experimental bifurcating jets, the combined axial and flapping forcing created a periodic array of vortex rings, which were alternatively shifted in the radial direction. The helical disturbances reached their maximum amplification at the end of the potential core. As a result, the rings tilted and propagated along two different trajectories. In our simulated jets, different 'bifurcating' mechanisms are revealed by the analysis of the space-time evolution of vortex structures.

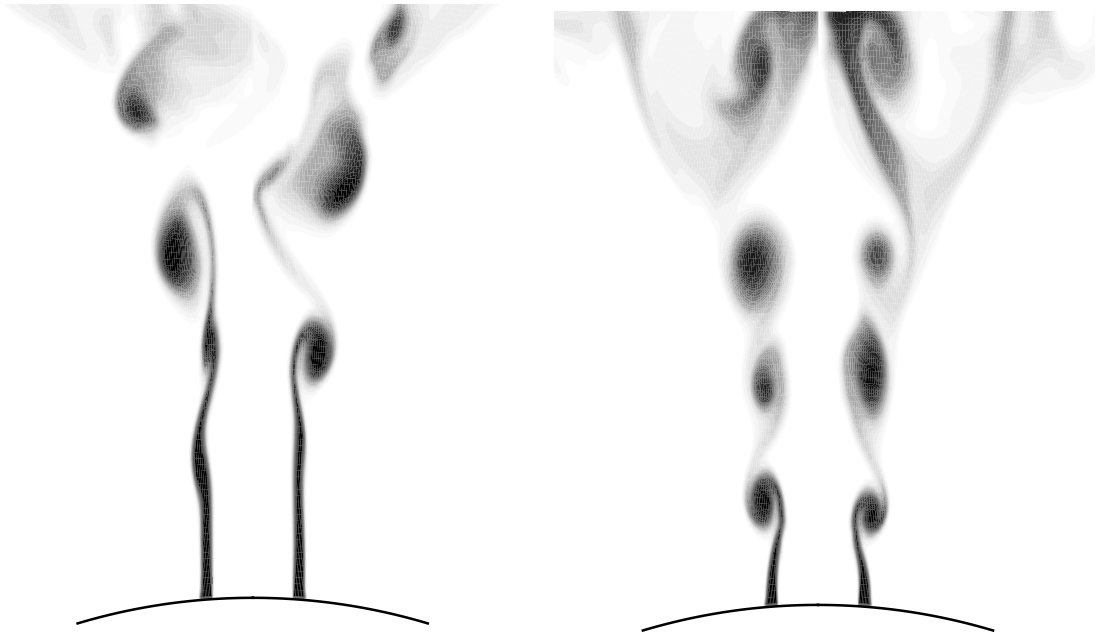

FIGURE 8. (F)-jet (left) and (BF)-jet (right). Instantaneous snapshot of the (S2) passive scalar field in the bifurcating plane ($\theta_c = 0$). Zoom near the nozzle.

Figures 8 and 9 offer a more detailed image of the large structures dominating the simulated jet flows. The near-field evolution of the (S2) tracer shows that flapping excitation delays the roll-up of the jet shear layer (Fig. 8-left). The first *cat-eyes* are formed at $z/D \approx 2.25$, compared to $z/D \approx 1.2$ for the (H)-jet. A greater percentage of the tracer is captured at azimuthal locations corresponding to maxima of the local velocity profile. At the diametrically opposite locations, weaker tracer filaments connect the staggered vortices at the azimuthal maxima. This observation is supported by the three-dimensional image of the coherent structures identified by means of iso-surfaces of low pressure (Fig. 9-left). Ring-like vortical structures roll up up in alternatively tilted planes every half-period of excitation. The core of these structures progressively diminishes towards the region of minimum perturbation amplitude. At this azimuthal location, the vortex ends do not merge in a toroidal loop. They bend downstream and merge with the next vortex, generating a large intertwined structure. This continuous structure breaks-up at $z/D \approx 5$. As a result, vortex structures similar to distorted rings propagate along two distinct branches. This last phase of vortex evolution is similar to that observed in experiments. However, the initial stages of formation of the involved 'ring' structures is different since we never observed the usual (see Fig. 5) toroidal rings in our simulation.

The shear-layer of the (BF)-jet rolls up into coherent vortex rings (Fig. 8-right) similar to those characterizing the axially excited jet (Fig. 4-left) except for the slight tilt of the vortices. The vortex pairing occurs at approximately the same downstream location. Farther downstream, the vortex ring undergoes strong azimuthal instabilities and finally break up into small and irregular vortex structures

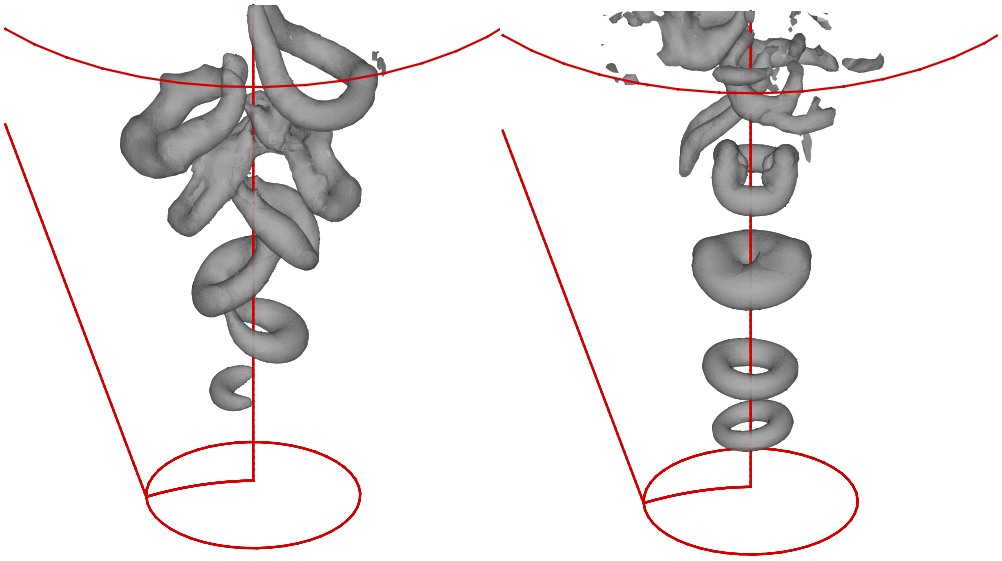

FIGURE 9. (F)-jet (left) and (BF)-jet (right). Identification of large coherent structures by instantaneous iso-surfaces of low pressure ($p = 0.2 \cdot p_{min}$).

(Fig. 9-right). As observed from Figs. 6 and 8, the flow abruptly spreads in the bifurcating plane before the complete destruction of the vortex rings. The tracer is ejected directly from the vortex sheet connecting the rings (braid region). This phenomenon can be explained by the excessive growth of streamwise filaments in the braid region (see Liepmann & Gharib 1992). The streamwise filaments are stretched by the high field strain and pulled outward from the jet by the moving vortex rings. The streamwise component of the vorticity vector is dominant in these regions (pictures not shown) and generates strong expulsion of passive tracer. In conclusion, the 'bifurcating' mechanism for the (BF)-jet concerns mainly the evolution of secondary streamwise vortice, rather than that of primary vortex rings. It should also be noted that the phase difference (Φ) between the axial and the flapping excitation (see Eq. 4) is essential to obtain bifurcation. The simulation with $\Phi = 0$ revealed small spreading in the excitation plan similar to that obtained for the (A)-jet.

4.3 Mean flow evolution

To assess if the behavior observed in the instantaneous pictures is highly repeatable, the mean flow fields were calculated. The statistical analysis is conducted within the same time period $T = 2D/(St_a \cdot V_0)$ for all the simulated cases. This period corresponds to the lowest forcing frequency ($\sim St_a/2$) used in the (BF)-case. The average procedure uses the information at every time step in the considered time interval. A converged mean flow field is obtained by averaging the mean data calculated for $2T$ time periods in the (A) and (H)-case and $4T$ time periods in the (F) and (BF)-case.

Figures 10 and 11 depict the mean fields of the (S1) scalar variable for all the simulated cases. The (A) and (H) jets display a very small spreading rate in all of the azimuthal planes. A dramatic increase of jet spreading in the bifurcating

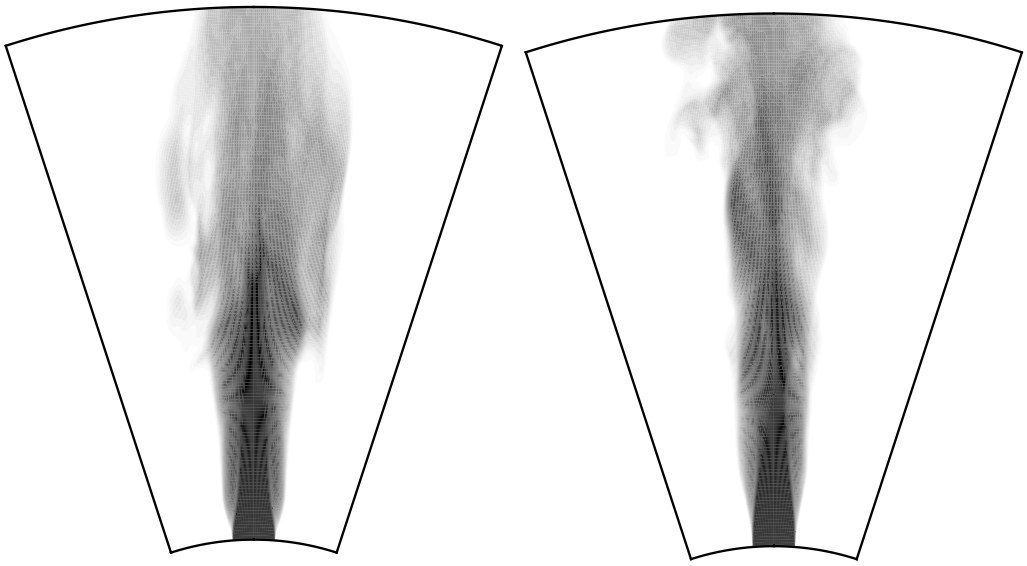

FIGURE 10. (A)-jet (left) and (H)-jet (right). Mean (S1) passive scalar field.

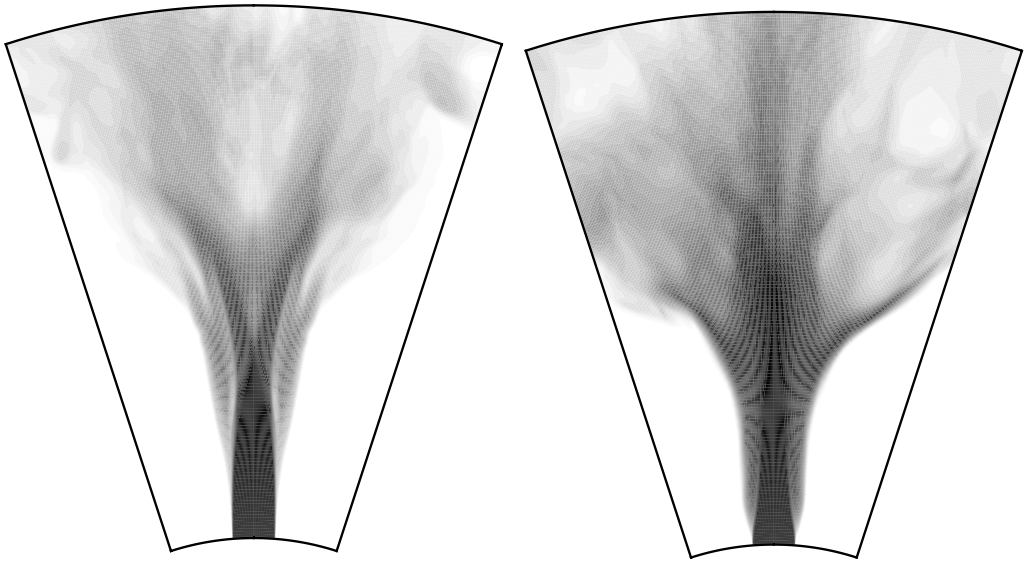

FIGURE 11. (F)-jet (left) and (BF)-jet (right). Mean (S1) passive scalar field in the bifurcating plane.

plane is observed for the (F) and (BF) cases. The Y-shaped structure of the (F)-jet (already observed in Fig. 6) is clearly displayed in this picture. Note the similarity with the pictures provided by the *product* visualizations in the bifurcating jets of Lee & Reynolds (1985). The (BF)-jet shows the greatest spreading rate. Although two distinct branches can be identified, the tracer concentration near the jet axis has a great value. The complicated *tree*-structure of the (BF)-jet can be generically described as Ψ-shaped. Based on these visualizations, we can speculate that the rapid breaking of the large structures in this jet enhances mixing and entrainment.

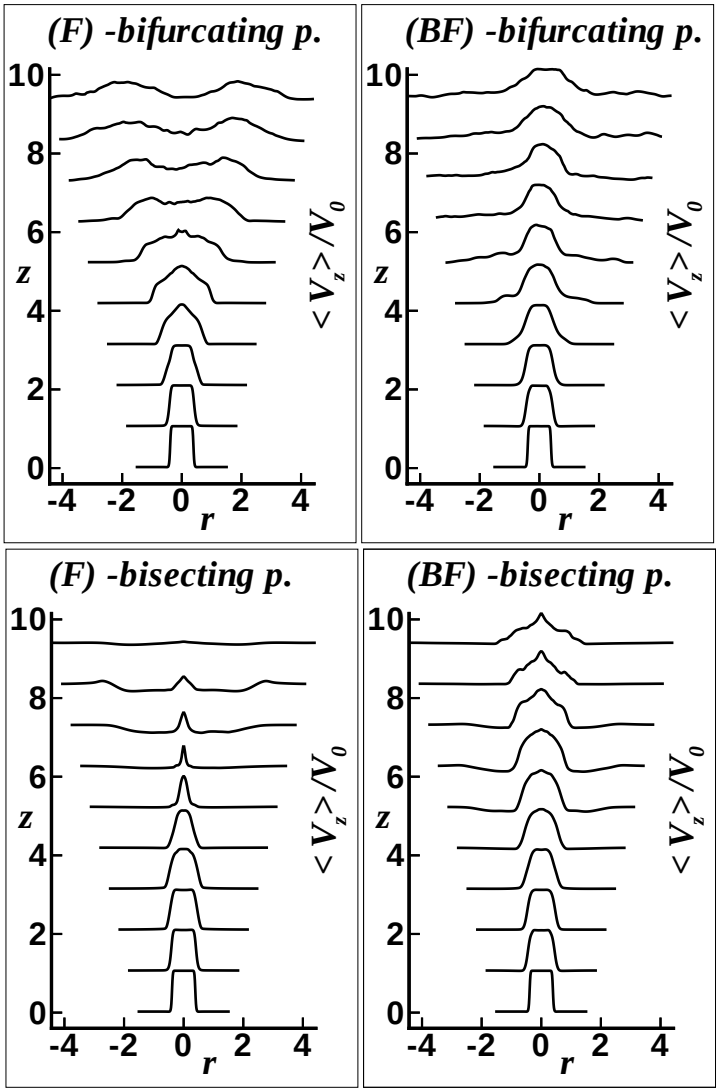

FIGURE 12. Mean streamwise velocity profiles for the (F) and (BF) jets.

Therefore, the (BF)-jet can be very interesting for practical applications.

The trends observed in the evolution of the (F) and (BF) jets can be summarized by plotting the mean streamwise velocity profiles (Fig. 12). In the far-region of the (F)-jet ($z/D \geq 5$), double-peak profiles can be observed in the bifurcating plane and very flat profiles in the bisecting plane. This evolution indicates that the jet flow splits into two distinct jets in the bifurcating plane and gradually vanishes in the perpendicular plane. The splitting of the jet main column in two branches directed in a well-defined azimuthal plane was reported as the most sticking feature of experimental bifurcating jets. The (BF)-jet displays a different evolution of the mean velocity. Bell-shaped profiles are observed in both bifurcating and bisecting planes. Nevertheless, the wider profiles in the bifurcating plane demonstrate the increased total momentum thickness and jet spreading in this plane.

5. Summary and final discussion

The evolution of a low Reynolds number round jet under periodic forcing was examined by means of DNS. The selection of the physical parameters of the spatial simulation was guided by the experimental studies of Lee & Reynolds (1985) and Parekh, Leonard & Reynolds (1988). The periodic forcing was numerically modeled by superposing streamwise velocity perturbations on the mean inflow velocity profile. The four considered types of perturbations represented linear combinations of the fundamental unstable modes in jets: (A) axisymmetric [$m = 0$], (H) helical [$m = 1$], (F) flapping [$(m = 1) + (m = -1)$], and (BF) bifurcating [$(m = 0) + (m = 1) + (m = -1)$].

The evolution of the axially and helically forced jets is in very good qualitative and quantitative agreement with previous theoretical and experimental studies. The flapping and the bifurcating perturbations generate jets with a spectacular increase of the spreading rate in the plane where the excitation locks (from 16^o for the (A)-jet to approximately. 90^o for the (BF)-jet).

In their attempt to semantically define bifurcating jets, Parekh *et al* (1988) emphasized that a jet which spreads more rapidly in one plane than in the perpendicular plane is not necessarily a bifurcating jet since elliptic jets exhibit the same characteristic. Based on flow-visualizations, they proposed two criteria to define a bifurcating jet: the jets split into two separate jets and/or the far-field streamwise velocity profiles consist of two separate peaks. The first criterion is fulfilled when the jet fluid disappears as one moves downstream in the plane perpendicular to the excitation plane.

The surprising result displayed in our simulations was that only the (F)-jet fulfilled the two criteria. The involved bifurcating mechanism was similar to that experimentally reported except for the formation of coherent ring-like structures. The (BF)-jet showed some similaritie, but also some clear differences when compared to experimental bifurcating jets. A new bifurcating mechanism based on the growth of secondary streamwise vortices was proposed to explain the observed behavior. Consequently, we propose a more general definition classifying a jet as bifurcating jet if it spreads rapidly in one plane but not in the perpendicular plane, without axis switching. This definition will exclude jets with non-circular nozzles (elliptic, triangular) and will include indeterminate-origin bifurcating jets.

Acknowledgments

We would like to acknowledge the helpful input of Prof. W. C. Reynolds and Prof. P. Moin in positioning this investigation. We also thank Prof. D. Parekh for stimulating discussions. The computing time on the IBM-SP2 was made available by the Maui High Performance Computing Center (MHPCC).

REFERENCES

Batchelor, G. K. & Gill, A. E. 1962 Analysis of the stability of axisymmetric jets. *J. Fluid Mech.* **14,** 529.

Boersma, B. J., Brethouver, G., & Nieuwstadt, F. T. M. 1998 A numerical investigation the effect of the inflow conditions on the self-similar region of a round jet. *Phys. Fluids.* **10,** 899.

Bouchard, E. E. Jr. & Reynolds, W. C. 1982 The role of large scale structures in the initial development of circular jets. *Report No. TF-17*, Department of Mechanical Engineering, Stanford University.

Bradbury, L. J. S. & Khadem, A. H. 1975 The distortion of a jet by tabs. *J. Fluid Mech.* **70,** 801.

Cohen, J. & Wygnanski, I. 1987 The evolution of instabilities in the axisymmetric jet. Part 1. The linear growth of disturbances near the nozzle. *J. Fluid Mech.* **176,** 191.

Cohen, J. & Wygnanski, I. 1987b The evolution of instabilities in the axisymmetric jet. Part 2. The flow resulting from the interaction between waves. *J. Fluid Mech.* **176,** 221.

Corke, T. C., Shakib, F., & Nagib, H. M. 1991 Mode selection and resonant phase locking in unstable axisymmetric jets. *J. Fluid. Mech.* **223,** 253.

Corke, T. C. & Kusek, S. M. 1993 Resonance in axisymmetric jets with controlled helical-mode input. *Fluid. Mech.* **249,** 307.

Crow, S. C. & Champagne, F. H. 1971 Orderly structure in jet turbulence. *J. Fluid Mech.* **48,** 547.

Danaila, I., Dusek J., Anselmet, F. 1998 Nonlinear dynamics at a Hopf bifurcation with axisymmetry breaking in a jet. *Phys. Rev. E.* **57,** 3696.

Danaila, I., Dusek J., Anselmet, F. 1997 Coherent structures in a round, spatially evolving, unforced, homogeneous jet at low Reynolds numbers. *Phys. Fluids.* **9,** 3323.

Dimotakis, P. E., Miake-Lie, R. C., & Papantoniou, D. A 1983 Structure and dynamics of round turbulent jets. *Phys. Fluids.* **26,** 3185.

Gresho, P. M. 1991 Incompressible fluid dynamics: Some fundamental formulations issues. *Ann. Rev. Fluid Mech.* **23,** 413.

Gutmark, G. & Ho, C. M. 1983 Preferred modes and the spreading rates of jets. *Phys. Fluids.* **26,** 2932.

Ho, C. M. & Huerre, P. 1984 Perturbed free shear layers. *Ann. Rev. Fluid Mech.* **16,** 365.

Ho, C. M. & Huang, L. S. 1982 Subharmonics and vortex merging in mixing layers. *J. Fluid Mech.* **119,** 443.

Huerre, P. & Monkewitz, P. A. 1990 Local and global instabilities in spatially developing flows. *Ann. Rev. Fluid Mech.* **22,** 473.

Hussain, A. K. M. F. & Zaman, Z. B. M. Q. 1980 Vortex pairing in a circular jet under control excitation. Part 2. Coherent structure dynamics. *J. Fluid Mech.* **101,** 493.

Hussain, A. K. M. F. & Clark, A. R. 1981 On the coherent structure of the axisymmetric mixing layer: a flow-visualization study. *J. Fluid Mech.* **104,** 263.

Jeong, J. & Hussain, F. 1995 On the identification of a vortex. *J. Fluid Mech.* **285,** 69.

Lasheras, J. C., Lecuona, A., & Rodriguez, P. 1991 Three-dimensional vorticity dynamics in the near field of coflowing forced jets. *Lect. Appl. Math.* **28,** 403.

Lee, M. & Reynolds, W. C. 1985 Bifurcating and blooming jets. *Report No. TF-22*, Department of Mechanical Engineering, Stanford University.

Liepmann, D. & Gharib, M. 1992 The role of streamwise vorticity in the near-field entrainment of round jets. *J. Fluid Mech.* **643.**

Longmire, E. K. & Duong, L. H. 1995 Bifurcating jets generated with stepped and sawtooth nozzles. *Phys. Fluids.* **8,** 978.

Lowery, P. S. & Reynolds, W. C. 1986 Numerical simulation of a spatially-developing, forced, plane mixing layer. *Report No. TF-26*, Department of Mechanical Engineering, Stanford University.

Mankbadi, R. R. & Liu, J. T. C. 1981 A study on the interactions between large scale coherent structures and fine-grained turbulence in a round jet. *Phil. Trans. R. Soc. Lond.* **A28,** 541.

Mattingly, G. E. & Chang C. C. 1974 Unstable waves on a axisymmetric jet column. *J. Fluid Mech.* **65,** 541.

Michalke, A. 1984 Survey on jet instability theory. *Prog. Aerospace Sci.* **21,** 159.

Morris, P. J. The spatial viscous instability of axisymmetric jets 1976. *J. Fluid Mech.* **77,** 511.

Morrison, G. L. & McLaughlin, D. K. 1980 Instability process in low Reynolds number supersonic jets. *AIAA J.* **18,** 793.

Orlanski, I. 1976 A simple boundary condition for unbounded hyperbolic flows. *J. Comp. Physics.* **21,** 251.

Parekh, D., Leonard, A., & Reynolds, W. C. 1988 Bifurcating jets at high Reynolds numbers. *Report No. TF-35*, Department of Mechanical Engineering, Stanford University.

Plaschko, P. 1979 Helical instabilities of slowly divergent jets. *J. Fluid Mech.* **92,** 209.

Webster, D. R. & Longmire, E. K. 1997 Vortex dynamics in jets from inclined nozzles . *Phys. Fluids.* **9,** 655.

Zaman, K. B. M. Q., Reeder, M. F., & Samimy, M. 1994 Control of an axisymmetric jet using vortex generators. *Phys. Fluids.* **6,** 778.

Zaman, K. B. M. Q. & Raman, G. 1997 Reversal in spreading of a tabbed circular jet under controlled excitation. *Phys. Fluids.* **9,** 3733.